Characterization of "dead-zone" eddies in the tropical Northeast Atlantic Ocean

Florian Schütte [1], Johannes Karstensen [1], Gerd Krahmann [1], Helena Hauss [1], Björn Fiedler [1],

Peter Brandt [1,2], Martin Visbeck [1,2] and Arne Körtzinger [1,2]

[1] GEOMAR Helmholtz Centre for Ocean Research Kiel, Germany

[2] Christian Albrechts University Kiel, Germany

Correspondence to: F. Schütte (fschuette@geomar.de)

Abstract

Localized open-ocean low–oxygen dead-zones in the tropical Northeast Atlantic are recently discovered ocean features that can develop in dynamically isolated water masses within cyclonic eddies (CE) and anticyclonic modewater eddies (ACME). Analysis of a comprehensive oxygen dataset obtained from gliders, moorings, research vessels and Argo floats revealed that eddies with low oxygen concentrations at 50-150 m depths can be found in surprisingly high numbers and in a large area (from about 4°N to 22°N, from the shelf at the eastern boundary to 38°W). Minimum oxygen concentrations of about 9 µmol kg^{-1} in CEs and severely suboxic concentrations (< 1 µmol kg^{-1}) in ACMEs were observed. In total, 173 profiles with oxygen concentrations below the minimum background concentration of 40 µmol kg^{-1} could be associated with 27 independent "dead-zone" eddies (10 CEs; 17 ACMEs) over a period of 10 years. The eddies' oxygen minimum is located in the eddy core beneath the mixed layer at a mean depth of 80 m. Compared to the surrounding waters, the mean oxygen anomaly between 50 and 150 m depth for CEs (ACMEs) is -38 (-79) µmol kg^{-1}. The low oxygen concentration right beneath the mixed layer has been attributed to the combination of high productivity in the eddies' surface waters and the isolation of their cores with respect to lateral oxygen supply. Indeed, eddies of both types feature a cold sea surface temperature anomaly and enhanced chlorophyll concentrations in their center. The locally increased consumption within these eddies represents an essential part of the total consumption in the open tropical Northeast Atlantic Ocean and might be partly responsible for the formation of the shallow oxygen minimum zone. Eddies south of 12°N carry weak hydrographic anomalies in their cores and seem to be generated in the open ocean away from the boundary. North of 12°N, eddies of both types carry anomalously low salinity water of South Atlantic Central Water origin from the eastern boundary upwelling region into the open ocean. Water mass properties and satellite eddy tracking both point to an eddy generation near the eastern boundary.

1. Introduction

The Eastern Tropical North Atlantic off northwest Africa (ETNA: 4°N to 22°N and from the shelf at the eastern boundary to 38°W, Fig. 1) is one of the biologically most productive areas of the global ocean (Chavez and Messié, 2009; Lachkar and Gruber, 2012). In particular, the eastern boundary current system close to the Northwest African coast is a region where northeasterly trade winds force coastal upwelling of cold, nutrient rich waters, resulting in high productivity (Messié et al., 2009). The ETNA region is characterized by a weak large-scale circulation (Brandt et al., 2015), but pronounced mesoscale variability (here referred to as eddies) acting as a major transport process between coastal waters and the open ocean (Schütte et al., 2015; Thomsen et al., 2015). In the ETNA, open ocean eddies with particularly high South Atlantic Central Water (SACW) fractions in their cores have been found offshore, where typically North Atlantic Central Water (NACW) dominates (Karstensen et al., 2015; Pastor et al., 2008). Due to low lateral mixing, SACW from the generation regions near the coast is trapped in the eddies' cores and transported offshore over long distances (Schütte et al., 2015). The impact of the eddy transport on the coastal productivity was investigated by Lachkar and Gruber (2012), who were able to show that high (low) eddy driven transports of nutrient-rich water from the shelf into the open ocean results in lower (higher) biological production on the shelf. Besides acting as export agents for coastal waters, coherent eddies in the ETNA have been reported to establish and maintain a sealed ecosystem (Fiedler et al., 2016; Hauss et al., 2015; Karstensen et al., 2015; Löscher et al., 2015). Coherent/isolated mesoscale eddies can exist over periods of several months or even years (Chelton et al., 2011). Enhanced vertical fluxes of nutrients and the dynamical isolation of the eddy interior from surrounding waters create very distinct biogeochemical conditions within these eddies, that can be very different from the surrounding water masses (Fiedler et al., 2016). Hypoxic to suboxic conditions have been observed in cyclonic eddies (CEs) and anticyclonic modewater eddies (ACMEs) caused by a combination of eddy dynamics and biogeochemical cycling within the eddies (Karstensen et al., 2015). The appearance of the low oxygen concentrations at shallow depth (about 50 to 100 m, just beneath the mixed layer) has been attributed to the combination of high productivity in the surface waters of the eddy, enhanced respiration of sinking organic material at subsurface depth and the isolation of the eddy core from the surrounding conditions. As such, these eddies resemble an environment similar to the "dead-zone" formation in coastal areas and lakes and therefore have been termed "dead-zone" eddies (Karstensen et al., 2015).

The ventilation and consumption processes of thermocline waters in the ETNA result in two separate oxygen minima (Fig. 1b): a shallow one with a core depth of about 80 m and a deep one at a core depth of about 450 m (Brandt et al., 2015; Karstensen et al., 2008). The deep minimum is the core of the OMZ and is primarily created by sluggish ventilation of the respective isopycnals (Luyten et al., 1983; Wyrtki, 1962). It extends from the eastern boundary into the open ocean and is located in the so-called shadow zone, with the more energetic circulation of the subtropical gyre in the north and the equatorial region in the south (Karstensen et al., 2008; Luyten et al., 1983). The shallow oxygen minimum intensifies from the equator towards the north with minimal values near the coast at about 20°N (Brandt et al., 2015) (Fig. 1a). It is assumed that the shallow OMZ originates from enhanced biological productivity and an increased respiration associated with sinking particles in the water column (Brandt et al., 2015; Karstensen et al., 2008; Wyrtki, 1962). In this paper we draw a connection between the enhanced consumption and associated low-oxygen concentration in "dead-zone" eddies and the formation of the regional observed shallow oxygen minimum zone. To assess the influence of "dead-zone" eddies on the oxygen budget of the upper water column, a sub-region between the ventilation pathways of the subtropical gyre and the zonal current bands of the equatorial Atlantic was chosen. This region includes the most pronounced

1   shallow oxygen minimum and is in the following referred to as shallow oxygen minimum zone (SOMZ, Fig. 1a).

2   The probability of "dead-zone" eddy occurrence per year is more or less evenly distributed in the ETNA (Fig.
3   1a). Particularly in the SOMZ there seems to be neither a distinctly high nor an explicitly low "dead-zone" eddy
4   occurrence. However, due to the absence of other ventilation pathways, the influence of "dead-zone" eddies on
5   the shallow oxygen minimum budget may be elevated and a closer examination worth the effort. The eddies in
6   this study were identified in 19 years of sea level anomaly (SLA) and sea surface temperature (SST) data based
7   on methods published by Schütte et al. (2015). After their formation near the eastern boundary, Rossby wave
8   dynamics and the basin scale circulation force eddies in the SOMZ to generally propagate westwards. The
9   dynamically protected eddy cores transport temperature, salinity, nutrient, carbon and oxygen conditions of their
10   formation region far offshore. At about 100 m depth, biogeochemical processes further increase the nutrient and
11   oxygen anomalies with respect to the surrounding waters. In order to further investigate the physical,
12   biogeochemical and ecological structure of dead-zone eddies, an interdisciplinary field study was carried out in
13   the ETNA, north of Cape Verde, using dedicated ship, mooring and glider surveys supported by satellite and
14   Argo float data. The analysis of the field study data revealed surprising anomalies in eddy meta-genomics
15   (Löscher et al., 2015), zooplankton (Hauss et al., 2015), carbon chemistry (Fiedler et al., 2016) and nitrogen
16   cycling (Karstensen et al. 2016). Furthermore, analyses of particle flux time series, using sediment trap data from
17   the Cape Verde Ocean Observatory (CVOO), were able to confirm the impact of highly productive dead-zone
18   eddies on deep local export fluxes (Fischer et al., 2015).

19   In this paper, we determine the average characteristics of "dead-zone" eddies in ETNA, addressing their
20   hydrographic features as well as occurrence, distribution, generation and frequency. Based on oxygen anomalies
21   and eddy coverage we estimate their contribution to the oxygen budget of the SOMZ. The paper is organized as
22   follows. Section 2 addresses the different in-situ measurements, satellite products and methods we use. Our
23   results are presented in section 3, discussed in section 4 and summarized in section 5.

25   **2. Data and methods**

26   **2.1 In-situ data acquisition**
27   For our study we employ a quality-controlled database combining shipboard measurements, mooring data and
28   Argo float profiles as well as autonomous glider data in ETNA. For details on the structure and processing of the
29   database, see Schütte et al. (2015). For this study we extended the database in several ways. The region was
30   expanded to now cover the region from 0° to 22° N and 13° W to 38° W (see Fig. 2). We then included data
31   from five recent ship expeditions (RV Islandia ISL_00314, RV Meteor M105, M107, M116, M119), which
32   sampled extensively within the survey region. Data from the two most recent deployment periods of the Cape
33   Verde Ocean Observatory (CVOO) mooring from October 2012 to September 2015 as well as Argo float data
34   for the years 2014 and 2015 were also included. Furthermore, oxygen measurements of all data sources were
35   collected and integrated into the database. As last modification of the database we included data from four
36   autonomous gliders that were deployed in the region and sampled two ACMEs and one CE. Glider IFM11
37   (deployment ID: ifm11_depl01) was deployed March 13, 2010. It covered the edge of an ACME on March 20
38   and recorded data in the upper 500 m. Glider IFM05 (deployment ID: ifm05_depl08) was deployed June 13,
39   2013. It crossed a CE on July 26 and recorded data down to 1000 m depth. IFM12 (deployment ID:

1   ifm12_depl02) was deployed January 10, 2014 north of the Cape Verde island São Vicente and surveyed

2   temperature, salinity and oxygen to 500 m depth. IFM13 (deployment ID: ifm13_depl01) was deployed on

3   March 18, 2014 surveying temperature, salinity and oxygen to 700 m depth. IFM12 and IFM13 were able to

4   sample three complete sections through an ACME. All glider data were internally recorded as a time series along

5   the flight path, while for the analysis the data was interpolated onto a regular pressure grid of 1 dbar resolution

6   (see also Thomsen et al., 2015). Gliders collect a large number of relatively closely spaced slanted profiles. To

7   reduce the number of dependent measurements, we limited the number of glider profiles to one every 12 hours.

8   The processing and quality control procedures for temperature and salinity data from shipboard measurements,

9   mooring data and Argo floats has already been described by Schütte et al. (2015). The processing of the gliders'

10 temperature and salinity measurements is described in Thomsen et al. (2015). Oxygen measurements of the

11 shipboard surveys were collected with Seabird SBE 43 dissolved oxygen sensors attached to Seabird SBE 9plus

12 or SBE 19 conductivity-temperature-depth (CTD) systems. Sampling and calibration followed the procedures

13 detailed in the GO-SHIP manuals (Hood et al., 2010). The resulting accuracies were ≤1.5 µmol kg^{-1}. Within the

14 CVOO moorings, a number of dissolved oxygen sensors (Aanderaa optodes type 3830) were used. The optodes

15 were calibrated at dedicated CTD casts and in the laboratory with water featuring 0% air saturation before

16 deployment and after recovery following the procedures described by Hahn et al. (2014). We estimate their

17 accuracies at <3 µmol kg^{-1}. A number of the Argo floats were equipped with oxygen sensors. As a full

18 calibration of these is usually not available, the measured data based on the factory calibration was included into

19 the database after a strict visual control removing suspicious profiles. The different manufacturers of Argo float

20 oxygen sensors specify their accuracy at least better than 8 µmol kg^{-1} or 5%, whichever is larger. Note that early

21 optodes can be significantly outside of this accuracy range, showing offsets of 15-20 µmol kg^{-1}, in some cases

22 even higher. All four autonomous gliders were equipped with Aanderaa optodes which were calibrated on

23 dedicated CTD casts following the procedures of Hahn et al. (2014). As gliders move through the water column

24 the oxygen measurements are not as stable as those from moored optodes analyzed by Hahn et al. (2014). We

25 thus estimate their accuracy to about 3 µmol kg^{-1}.

26

27 As final result the assembled in-situ database of the ETNA contains 15059 independent profiles (Fig. 2). All

28 profiles include temperature, salinity and pressure measurements while some 38.5% include oxygen

29 measurements. The total number is composed of 13% shipboard, 22.5% CVOO mooring, 63% Argo float and

30 1.5% glider profiles. To determine the characteristics of different eddy types from the assembled profiles, we

31 separated them into anticyclones, CEs, ACMEs and the "surrounding area" not associated with eddy-like

32 structures following the approach of Schütte et al. (2015).

33

34 **2.2 Satellite data**

35 We detected and tracked eddies following the procedures described in Schütte et al. (2015). In brief we used the

36 delayed-time reference dataset of Sea Level Anomaly (SLA; version 2014). The data is produced by

37 Ssalto/Duacs and distributed by AVISO (Archiving, Validation, and Interpretation of Satellite Oceanographic),

38 with support from CNES [http://www.aviso.altimetry.fr/duac/]. We used the multi-mission product, which is

39 mapped on a 1/4° x 1/4° Cartesian grid and has a temporal resolution of one day. The anomalies were computed

40 with respect to a twenty-year mean. Data of the SLA and of the geostrophic velocities, derived from the SLA

41 and also provided from AVISO, for the period January 1998 to December 2014 were chosen.

1   For Sea Surface Temperature (SST) the dataset "Microwave Infrared Fusion Sea Surface Temperature" from
2   Remote Sensing Systems (www.remss.com) is used. It is a combination of all operational microwave (MW)
3   radiometer SST measurements (TMI, AMSR-E, AMSR2, WindSat) and infrared (IR) SST measurements (Terra
4   MODIS, Aqua MODIS). The dataset thus combines the advantages of the MW data (through-cloud capabilities)
5   with the IR data (high spatial resolution). The SST values are corrected using a diurnal model to create a
6   foundation SST that represents a 12-noon temperature (www.remss.com). Daily data with 9 km resolution from
7   January 2002 to December 2014 is considered.
8   For sea surface chlorophyll data (Chl) we use the MODIS/Aqua Level 3 data available at
9   http://oceancolor.gsfc.nasa.gov provided from the NASA. The data is measured via IR and is therefore cloud
10 cover dependent. Daily data mapped on a 4 km grid from January 2006 to December 2014 is selected.

12 **2.3 "Dead-zone" eddy detection and surface composites**
13 In order to verify whether low oxygen concentrations (<40 µmol kg^{-1}) at shallow depth (above 200 m) are
14 associated with eddies we applied a two step procedure: First, all available oxygen measurements of the
15 combined in-situ datasets are used to identify low oxygen values. Next, the satellite data based eddy detection
16 results (Schütte et al., 2015) were matched in space and time with the location of anomalously low oxygen
17 profiles. In this survey the locations of 173 of the 180 low oxygen profiles coincide with surface signatures of
18 mesoscale eddies. Schütte et al. (2015) showed that ACMEs can be distinguished from normal anticyclonic
19 eddies by considering the SST anomaly (cold in case of ACMEs) and SSS anomaly (fresh in case of ACMEs) in
20 parallel to the respective SLA anomaly. The satellite based estimates of SLA and SST used in this study are
21 obtained by subtracting low-pass filtered (cutoff wavelength of 15° longitude and 5° latitude) values from the
22 original data to exclude large-scale variations and preserve only the mesoscale variability (see Schütte et al. 2015
23 for more detail). All eddy-like structures with low oxygen profiles are visually tracked in the filtered SLA
24 (sometimes SST data) back- and forward in time in order to obtain eddy propagation trajectories. The surface
25 composites of satellite-derived SLA, SST and Chl data consist of 150 km x 150 km snapshots around the
26 obtained eddy centers. For construction of the composites the filtered SLA and SST is used as well.
27

28 **2.4 Reconstruction of oxygen concentrations in "dead-zone" eddy cores**
29 About 30 % of the profiles from the combined in-situ dataset conducted in CEs or ACMEs do not have oxygen
30 measurements available. However, we are only interested in oxygen measurements in isolated CE or ACME
31 cores. These isolated eddy cores carry anomalously low salinity SACW of coastal origin in their cores, while the
32 surrounding waters are characterized by an admixture of more saline NACW (Schütte et al., 2015). The fresh
33 cores indicate a generation site near the coast and strong isolation due to reduced lateral mixing with the more
34 saline surrounding waters during their westward migration into the open ocean. Due to this strong isolation and
35 an intensified biogeochemical cycling within the eddies, the oxygen content in the eddy cores decreases rapidly
36 (Karstensen et al., 2015). The salinity-σ_θ diagram (Fig. 3a) based on the profiles with oxygen measurements
37 indicates that low saline waters in the eddy cores are related to low oxygen concentrations (considering here only
38 eddies which are located in the open ocean, west of 19°W). To compensate for missing oxygen measurements a
39 salinity-oxygen relation in combination with isolation time and associated oxygen consumption within the eddy
40 cores was derived. To assess the consumption within the eddies, an average oxygen utilization rate per day based
41 on the available oxygen measurements is derived for both eddy types. In detail, the distance of the eddy to the

1 eastern boundary and the associated propagation time is derived We assume a mean westward eddy propagation

2 of 3 km d^{-1} (Schütte et al., 2015). Further we assume a typical oxygen profile at the eastern boundary (mean of

3 all profiles east of 18°W) as initial oxygen condition in the eddy core (see Fig. 3b). The mean eddy consumption

4 rate is now the difference from the initial oxygen condition and the actual oxygen concentration in the eddy core

5 divided by the propagation time. If an eddy without oxygen measurements and SACW water mass characteristics

6 (less saline and colder water than the surrounding water) is identified we assume a strong isolation of the eddy.

7 Using the consumption rates of isolated CEs and ACMEs and the associated propagation time a reconstructed

8 oxygen value within the eddy could be derived. Using this method, oxygen values could be constructed for all

9 profiles within CEs or ACMEs, even if only salinity and temperature measurements are available. To validate

10 the method we reconstruct oxygen profiles for the eddies with available oxygen measurements and compared

11 them (Fig. 3b). An average uncertainty of ±12 (16) µmol kg^{-1} is associated with the reconstructed oxygen values

12 (Fig. 3c) of CEs (ACMEs). This uncertainty is even higher in the core region of the eddies. Depending on the

13 status of isolation of the eddy lateral mixing could take place, which is assumed to be zero in our method.

14 However, this approach enables us to enlarge the oxygen dataset by 30%. In this paper the reconstructed oxygen

15 values are only used for the derivation of the mean vertical oxygen anomaly.

17 **2.5 Mean vertical oxygen anomaly of "dead-zone" eddies and their impact on the SOMZ**

18 To illustrate mean oxygen anomalies for CEs and ACMEs as a function of depth and radial distance, all oxygen

19 profiles (observed and reconstructed) were sorted with respect to a normalized distance, which is defined as the

20 actual distance of the profile from the eddy center divided by the radius of the eddy (the shape and thus the

21 radius of the eddy are gained from the last closed contour of the geostrophic surface velocity). The oxygen

22 profiles were grouped and averaged onto a grid of 0.1 increments between 0 and 1 of the normalized radial

23 distance. Finally a running mean over three consecutive horizontal grid points was applied. A mean oxygen

24 anomaly for the CEs and the ACMEs was constructed by the comparison with the oxygen concentrations in the

25 surrounding waters. To illustrate the influence of the reconstructed oxygen values, the mean vertical oxygen

26 anomaly is also constructed based only on original measured oxygen values, both anomalies are shown for

27 comparison.

28

29 An oxygen deficit profile due to "dead-zone" eddies in the SOMZ is derived by building an oxygen anomaly of

30 each eddy type on density surfaces (O_2'). The derived anomalies are multiplied by the mean number of eddies

31 dissipating in the SOMZ per year (n) and weighted by the area of the eddy compared to the total area of the

32 SOMZ (A_{SOMZ} = triangle in Fig. 1a). Differences in the mean isopycnal layer thickness of each eddy type and

33 the SOMZ are considered by multiplying the result with the ratio of the mean Brunt-Väisälä frequency (N^2)

34 outside and inside the eddy, resulting in an apparent oxygen utilization rate per year (µmol kg^{-1} y^{-1}) due to "dead-

35 zone" eddies in the SOMZ on density layers:

36

$$aOUR = nO_2' \frac{\pi r_{Eddy}^2 N_{SOMZ}^2}{A_{SOMZ} N_{Eddy}^2}$$

37

38 where r_{Eddy} is the mean radius of the eddies.

39

1 **3. Results**

2 **3.1 Low oxygen eddy observation from in-situ data**

3 Several oxygen measurements with anomalously low oxygen concentrations for the ETNA region (below 40

4 µmol kg^{-1} at shallow depth) could be identified from Argo floats, ship surveys, glider missions and from the

5 CVOO mooring (Fig. 4). In total, 27 independent eddies with oxygen values <40 µmol kg^{-1} in the upper 200 m

6 were sampled with 173 profiles from 25 different platforms (Tab. 1). Almost all of the observed anomalous low

7 oxygen values could be associated with mesoscale structures at the sea surface (CEs or ACMEs) from satellite

8 data.

9 In-situ measurements for meridional velocity, temperature and oxygen of the CVOO mooring during the

10 westward passage of one CE and one ACME with low oxygen concentrations are chosen to show examples of

11 the vertical structure of the two different eddy types based on temporally high resolution data (Fig. 5). From

12 October 2006 to December 2006 (Fig. 5a), a 65 km diameter CE passed the CVOO mooring position on a

13 westward trajectory. At its closest the eddy center was located 20 km north of the CVOO mooring. The

14 meridional velocities show a strong cyclonic rotation (first southward, later northward) with velocity maxima

15 between the surface and 50 m depth at the edges of the eddy. In the core of the CE, the water mass was colder

16 and less saline (not shown) than the surrounding water, the mixed layer (ML) depth is reduced and the

17 isopycnals are shifted upwards. The oxygen content of the eddy core was decreased with values around 60

18 µmolkg^{-1} at 115 m depth (or at the isopycnal surface 26.61 kg m^{-3}) compared to surrounding waters, which have

19 a mean (± 1 standard deviation) oxygen content of 113 (±38) µmol kg^{-1} at around 150 m depth or 26.60 (±0.32)

20 kg m^{-3} during the mooring period between 2006 to 2014.

21 From January 2007 to March 2007 (Fig. 5b), an ACME passed the CVOO mooring position. The core of the

22 westward eddy passed 13 km to the north of the mooring. The velocity field shows strong subsurface

23 anticyclonic rotation at the depths of the core between 80-100 m depth. In contrast to other typical anticyclonic

24 eddies, the water mass in the eddy core of the ACME is colder and less saline (not shown) than the surrounding

25 waters. The isopycnals above the core are elevated resulting in shallower MLs both resembling a cyclone.

26 Beneath the core, the isopycnals are strongly depressed as in a "normal" anticyclone. Thus, dynamically this

27 resembles a mode water anticyclone, an eddy type, which is e.g. well-known from the Mediterranean outflow

28 regime (Bower et al., 1995; Richardson et al., 1989). In contrast to the historical known mode water

29 anticyclones, the eddy core is shallower (just beneath the ML) and therefore the oxygen concentration is

30 reduced. The oxygen content in the eddy's core recorded from the CVOO mooring is strongly decreased with

31 values around 19 µmol kg^{-1} at 123 m depth (or 26.50 kg m^{-3}) compared to the surrounding waters (113 (±38)

32 µmol kg^{-1}). Within the entire time series, the CVOO mooring recorded the passage of several ACMEs with even

33 lower oxygen concentrations (for more information see Karstensen et al. (2015) or Table 1).

34

35 **3.2 Combining in-situ and satellite data for "dead-zone" eddy detection in the ETNA**

36 Combining the location and time of in-situ detection of low oxygen eddies with the corresponding SLA satellite

37 data reveals a clear link to the surface manifestation of mesoscale structures, CE and ACMEs likewise (Fig. 4).

38 Composite surface signatures for SLA, SST and Chl from all identified anomalous low oxygen eddies from the

39 in-situ data are shown in Figure 6. The composites for ACMEs are based on 17 independent eddies and on 922

40 surface maps. The detected ACMEs are characterized by an elevation of SLA, which is associated with an

41 anticyclonic rotation at the sea surface. The magnitude of the SLA displacement is moderate compared to normal

1   anticyclones and CEs (Schütte et al., 2015). More distinct differences to normal anticyclones are the cold-water

2   anomaly and the elevated Chl concentrations in the eddy center of the ACMEs. Normal anticyclones are

3   associated with elevated SST and reduced Chl concentrations. Through a combination of the different satellite

4   products (SLA, SST, SSS) it is possible to determine "dead-zone" eddies from satellite data alone (further details

5   in Schütte et al. (2015)).

6   The composite mean surface signature for "dead-zone" CEs is based on 10 independent eddies and on 755

7   surface maps. The CEs are characterized by a negative SLA and SST anomaly. The observed negative SST

8   anomaly of the "dead-zone" CEs is twice as large (core value CE: -0.12 ±0.2 °C; core value ACME: -0.06 ±0.2

9   °C) as the corresponding anomaly of the ACMEs. The Chl concentration in the eddy center is also higher for

10   CEs compared to ACMEs (core value CE: 0.35 ±0.22 log mg m^{-3}; core value ACME: 0.21 ±0.17 log mg m^{-3}).

11   Note, that we only considered the measured low oxygen ACMEs and CEs from Table 1 to derive the composites.

13   Using the eddy-dependent surface signatures in SLA, SST and Chl the "dead-zone" eddies could be tracked and

14   an eddy trajectory could be derived (e.g. Fig. 4). All detected eddies were propagating westward into the open

15   ocean. North of 12°N, most of the eddies set off near the coast, whereas south of 12°N the eddies seem to be

16   generated in the open ocean. Detected CEs have a tendency to deflect poleward on their way into the open ocean

17   (Chelton et al., 2011), whereas ACMEs seem to have no meridional deflection. However, during their westward

18   propagation the oxygen concentration within the "dead-zone" eddy cores decreases with time. Using the

19   propagation time and an initial coastal oxygen profile (Fig. 3b) a mean apparent oxygen utilization rate per day

20   could be derived for all sampled eddies (Fig. 7). On average the oxygen concentration in the core of an isolated

21   CE (ACME) decreases by about 0.10 (0.19) ± 0.12 (0.08) µmol kg^{-1} d^{-1}.

23 3.4 Mean oxygen anomalies from "dead-zone" eddies in the ETNA

24   In Figure 8 we compare the mean oxygen anomalies based purely on observations with those based on the

25   extended profile database including observed and reconstructed oxygen values (see section 2.4). It shows the

26   mean oxygen anomalies against the surrounding water for CE (Fig. 8a) and ACME (Fig. 8b) versus depth and

27   normalized radial distance. On the left side of each panel the anomaly is based on the in-situ and reconstructed

28   oxygen values (736 oxygen profiles; 575 in CEs; 161 in ACMEs), whereas on the right side the anomaly is based

29   only on the in-situ oxygen measurements (504 oxygen profiles; 395 in CEs; 109 in ACMEs). The distinct mean

30   negative oxygen anomalies for CEs and ACMEs indicate the low oxygen concentrations in the core of both eddy

31   types compared to the surrounding water. The strongest oxygen anomalies are located in the upper water

32   column, just beneath the ML. CEs feature maximum negative anomalies of around -100 µmol kg^{-1} at around 70

33   m depth in the eddy core, with a slightly more pronounced oxygen anomaly on the left part including the

34   reconstructed values compared to the right part based only on observed oxygen concentrations (Fig. 8a). This is

35   contrary for the ACME with stronger oxygen anomalies on the right part than on the left (Fig. 8b). Both methods

36   deliver maximum negative anomalies of around -120 µmol kg^{-1} at around 100 m depth in the ACME core. At

37   that depth, the diameter of the mean oxygen anomaly is about 100 km for ACMEs and 70 km for CEs. Beneath

38   150 m depth, magnitude and diameter of the oxygen anomalies decrease rapidly for both eddy types. Figure 8c is

39   based on both, the in-situ and reconstructed oxygen values, and shows the horizontal mean oxygen anomaly

40   profile of each eddy type against depth obtained by horizontally averaging the oxygen anomalies shown in Fig.

41   8a,b. The maximum anomalies are -100 µmol kg^{-1} at around 90 m for ACMEs and -55 µmol kg^{-1} at around 70 m

1   for cyclones. Both eddy types have the highest oxygen variance directly beneath the ML (in the eddy core) or

2   slightly above the eddy core. The oxygen anomaly (and associated variance) decreases rapidly with depth

3   beneath the eddy core and is smaller than around -10 ± 10 µmol kg^{-1} beneath 350 m for both eddy types.

5   **4. Discussion**

6   The minimum oxygen concentrations for ETNA between the surface and 200 m depth (Fig. 1) from the MIMOC

7   climatology (Schmidtko et al., 2013) illustrates that oxygen values below 50 µmol kg^{-1} are not a common feature

8   of the large scale oxygen field in the ETNA. However, oxygen concentrations below the canonical value of 40

9   µmol kg^{-1} (Stramma et al., 2008) are found in oxygen profiles taken from various observing platforms (ships,

10   moorings, floats) and could nearly entirely be co-located with mesoscale features. In the current analysis we

11   could identify 27 independent low oxygen eddies (10 CEs and 17 ACMEs) from our database. Eddies are

12   defined as coherent structures with a lifetime of several weeks to more than a year (Chelton et al., 2007).

13   Although the ETNA is expected to have a low activity of long-lived eddies (Chaigneau et al., 2009; Chelton et

14   al., 2011), we could identify 234 CEs and 18 ACMEs per year in the ETNA with a radius > 45 km and a tracking

15   time of more than 3 weeks. For eddy detection we used an algorithm based on the combination of the Okubo-

16   Weiß method and a modified version of the geometric approach from Nencioli et al. (2010) with an adjusted

17   tracking for the ETNA (for more information see Schütte et al. (2015)). Tracking ACMEs in SLA data was

18   rather difficult due to the small signal to noise ratio (not the case for the CEs), which led to a failure of the

19   automatic tracking algorithms in most cases. However, we used other satellite data in parallel (Fig. 6). As

20   discussed in Schütte et al. (2015) in case of coincidence of low SST and low sea surface salinity (not shown

21   here) as well as intense near surface phytoplankton blooms (Karstensen et al. 2015) we expected a high

22   likelihood that a low oxygen eddy was present. Note, all tracks of ACMEs and CEs shown in Figure 4 were

23   visually verified. The weak surface signature of ACMEs suggests that their frequency of occurrence might be

24   underestimated (e.g. in Schütte et al. (2015) but also in other studies). Moreover, we identified a few occurrences

25   of ACMEs based on shipboard ADCP as well as hydrographic measurements (e.g. during the research cruises of

26   Ron Brown 2009 and Meteor 119) that did not have a significant SLA signature.

27   Anticyclonic rotating eddies with a low oxygen core are only observed for modewater type anticyclones (i.e.

28   ACMEs), but not for "normal" anticyclonic eddies. We could show here that the ACMEs and CEs with a low

29   oxygen core tend to have also anomalous water mass properties (cold and fresh). In summary, the heat, salt, and

30   oxygen anomalies of ACMEs in the ETNA are fundamentally different (cold/fresh) from normal anticyclones

31   (warm/salty) (Schütte et al. 2015). Consequently a further distinction into the two types of anticyclonic eddies in

32   global (Chelton et al., 2011; Zhang et al., 2013) as well as regional eddy assessments is necessary.

33   It has been shown that the low-oxygen eddies in the ETNA could be separated into two different regimes, north

34   and south of 12°N (Fig. 4). The eddies north of 12°N are generally generated along the coast and in particular

35   close to the headlands along the coast. Schütte et al. (2015) suggested that these eddies are generated from

36   instabilities of the northward directed alongshore boundary current. However, the detailed formation processes

37   need to be further investigated. The formation of the eddies south of 12°N needs to be further investigated as

38   well, because their generation, dynamics and water mass anomalies are different from the ACMEs in the north.

39   The southern eddies do transport low-oxygen anomalies, but do not originate from a coastal boundary upwelling

40   system. Following the trajectories it seems that the ACMEs are generated in the open ocean between 5°N and

41   7°N. The generation mechanism could be related to the presence of strong tropical instabilities in that region

1 (Menkes et al., 2002; von Schuckmann et al., 2008).

2 As the "northern" and "southern" eddies have different generation mechanisms and locations as well as different

3 characteristics they need to be discussed separately. The core of the eddies generated north of 12°N is

4 characterized by less saline and cold SACW (Schütte et al., 2015) and thereby forms a strong hydrographic

5 anomaly against the background field. On the contrary, the core of the eddies generated south of 12°N does not

6 show any significant hydrographic anomalies. However, both eddy regimes feature eddies which generate during

7 their westward propagation locally open ocean upwelling systems with high productivity at the surface and

8 enhanced respiration beneath the ML (Karstensen et al., 2016). In combination with the eddy dynamics and its

9 associated isolation of the CE (ACME) core, the oxygen content is decreasing on average by about 0.10 (0.19) ±

10 0.12 (0.08) µmol kg^{-1} d^{-1} in the ETNA. The apparent oxygen utilization rate (aOUR) is based on 504 oxygen

11 measurements in CEs and ACMEs. It is in the range of recently published aOUR estimates for CEs (Karstensen

12 et al., 2015) and ACMEs (Fiedler et al., 2016) based on single measurements in "dead-zone" eddies. An

13 important point regarding the method to derive the aOURs is the initial coastal oxygen concentration, which is

14 highly variable in coastal upwelling regions (Thomsen et al., 2015). However, all observed CEs or ACMEs

15 contain a negative oxygen anomaly, partly because they transport water with initial low oxygen concentrations

16 from the coast into the open ocean and additionally because the oxygen consumption in the eddies is more

17 intense then in the surrounding waters (Karstensen et al. 2015a, Fiedler et al. 2015). Due to the smaller Coriolis

18 parameter closer to the equator the southern eddies should be more short-lived compared to eddies north of 12°N

19 (Chelton et al., 2011). This would suggest that, to achieve similarly strong negative oxygen anomalies, the

20 oxygen consumption in the eddies south of 12°N must be even stronger than in the ACMEs further north.

21 Pronounced productivity patterns in tropical instability waves and vortices have been reported in the past

22 (Menkes et al., 2002), but were not connected to low oxygen eddies before.

24 The mean oxygen profiles from the coast and inside of all CEs and ACMEs (Fig. 3b) indicate no pronounced

25 oxygen difference beneath 250 m depth. The largest anomalies have been observed in the eddy cores at around

26 100 m depth (Fig. 8). As a result of the dynamic structure, the core water mass anomalies of the ACMEs are

27 more pronounced than the one of the CE (Karstensen et al. 2016) and consequently the oxygen anomalies are

28 stronger. This is supported by the differences in the oxygen anomaly based on the measured plus reconstructed

29 and the measured oxygen values. The reconstruction of oxygen values assumes a complete isolation of the eddy

30 core. The left side of Figure 8, which includes the reconstructed oxygen values, features a larger oxygen

31 anomaly than the right side based on measured oxygen values only. Consequently the CEs seem to be not

32 completely isolated and the evolving oxygen anomaly is affected by low lateral mixing. On the contrary, the

33 oxygen anomaly of ACMEs is smaller for the reconstruction than for the measured oxygen values. It seems that

34 the ACMEs are more effectively isolated resulting in enhanced apparent consumption in the ACME core. One

35 should mention, however, that one possible error source of the reconstructed oxygen values could be the

36 assumption of a linear decrease of oxygen with time.

37

38 In the following, an estimate of the contribution of the negative oxygen anomalies of "dead-zone" eddies to the

39 oxygen distribution of the SOMZ is presented. The SOMZ is located west of the boundary current coastal

40 region, south of the subtropical gyre region and north of the zonal equatorial current bands. It covers the

41 unventilated eastern boundary shadow zone and thereby is the region of the most pronounced shallow oxygen

1   minimum (see Fig. 1a). The satellite-based eddy tracking reveals that on average 14 (2) CEs (ACMEs) each year

2   are propagate from the upwelling system near the coast into the SOMZ and dissipate here. By deriving the

3   oxygen anomaly on density surfaces an oxygen loss profile due to "dead-zone" eddies in the SOMZ is derived

4   (Fig. 9). Note that due to the lower oxygen values within the eddies compared to the surrounding waters in the

5   SOMZ, the release of negative oxygen anomalies to the surrounding waters is equivalent to a local (eddy

6   volume) enhancement of the oxygen utilization by -7.35 (-2.41) μmol kg^{-1} yr^{-1} for CEs (ACMEs) for the depth

7   range of the shallow oxygen minimum in the SOMZ, i.e. 50 to 150 m depth.

8   An equivalent view is, by investigating a simple mix ratio of higher with lower oxygen waters in a box model

9   approach of the SOMZ. When averaging the oxygen concentrations of the eddies in the considered depth range,

10   i.e. 50 to 150 m depth, a mean oxygen concentration of 73 (66) μmol kg^{-1} for CEs (ACMEs) is derived. The

11   background field oxygen concentration (118 μmol kg^{-1}, averaged over the same depth range between 50 and 150

12   m depth derived from the MIMOC climatology Schmidtko et al. (2013)) includes the effect of low oxygen

13   eddies. Considering the respective oxygen concentrations and volumes of the SOMZ and the eddies (multiplied

14   by their frequency of occurrence per year), we estimate the theoretical background oxygen concentration for the

15   SOMZ without eddies to 125 μmol kg^{-1}. Naturally due to the dispersion of negative oxygen anomalies, the

16   oxygen concentrations in the SOMZ without eddies must be higher than the observed values. Attributing the

17   difference of these values (oxygen concentration respiration without eddies (125 μmolkg^{-1}) and observed values

18   with eddies (118 μmolkg^{-1}) solely decreased due to the dispersion of eddies, we find that around 6% of the

19   observed oxygen concentrations in our box model can be associated to the dispersion of eddies. Consequently,

20   the oxygen consumption in the region is a mixture of the large-scale metabolism in the open ocean (Karstensen

21   et al. 2008) and the enhanced metabolism in low oxygen eddies (Karstensen et al. 2016, Fiedler et al. 2015). This

22   estimates should be considered as a lower limit due to the problems in detecting and tracking ACMEs (weak

23   SLA anomaly) and the assumption of zero lateral ventilation within the eddies. The real amount of "dead-zone"

24   eddies dissipate in the SOMZ is probably higher as only eddies which could be followed with tracking

25   algorithms directly from the coast into the transition zone and have a greater radius than 45 km and a lifetime

26   more than 21 days are considered.

27   This additional respiration term can be important in numerical simulations, where up to now only the large scale

28   consumption is taken into account. These results question the assumption that the oxygen consumption is

29   determined by the metabolism of the large-scale community alone. The observations presented here suggest

30   instead that hot spots of locally enhanced consumption may possibly need to be considered in the future.

31

32   **5. Conclusion**

33   In this study, we investigated the vertical structure of oxygen depleted eddies in the ETNA based on satellite (a

34   combination of SLA and SST) and in-situ oxygen and hydrography data (ship data, mooring data, profiling

35   floats, underwater glider). We frequently detected oxygen concentrations below the canonical value of 40 μmol

36   kg^{-1} within the ETNA that are associated with CEs and ACMEs. Lowest oxygen concentration in these eddies

37   was observed at shallow depth between 50 to 150 m. Both eddy types are characterized by a positive Chl

38   anomaly, and therefore the enhanced productivity and subsequent respiration of the organic material is

39   responsible for creating the low oxygen core during the westward propagation of these eddies from their

40   formation region along the West African coast into the open ocean. Our assessment reveals that 234 CEs (18

1 ACMEs) are generated each year (mostly on the eastern side) in the ETNA and can be tracked longer than 3

2 weeks, which here are considered as coherent eddies. On average the oxygen concentration in the core of such an

3 isolated CE (ACME) decreases by about 0.10 (0.19) ± 0.12 (0.08) μmol kg^{-1} d^{-1}. Beside the eddies originating in

4 formation regions along the West African coast, we observe low oxygen eddies (primarily ACMEs) relatively

5 close to the equator, south of 12°N. These eddies may be generated from flow instability processes occurring

6 during the formation of tropical instability waves.

7 However, both types of eddies (north of 12°N and south of 12°N) contain their minimum oxygen concentration

8 in the depth range where a shallow oxygen minimum is found in ETNA. The additional consumption within

9 these low oxygen eddies represents a substantial part of the total consumption in the open ETNA and might be

10 partly responsible for the formation of the shallow oxygen minimum.

12 **Acknowledgements**

13 This study was funded by the Deutsche Bundesministerium für Bildung und Forschung (BMBF) as part of the

14 project AWA (01DG12073E), by the Deutsche Forschungsgemeinschaft through the Collaborative Research

15 Centre "SFB 754" and several research cruises with RV Meteor, RV Maria S. Merian, Ronald H. Brown and RV

16 L'Atalante. Furthermore by the Cluster of Excellence "The Future Ocean" (CP1341), the project "Eddy-Hunt"

17 (CP1341) and the BMBF project SOPRAN (03F0611A and 03F0662A). The CVOO mooring is part of the

18 OceanSITES mooring network. The captains and the crew of the research vessels and our technical group for

19 their help with the fieldwork deserve special thanks. Furthermore the authors thank Tim Fischer for continuing

20 support and discussion and Rebecca Hummels for proof reading and for assisting in improving this paper.

21 The Argo data using in this study were collected and made freely available by the International Argo Program

22 and the national programs that contribute to it. (http://www.argo.ucsd.edu, htpp://argo.jcommops.org). The Argo

23 Program is part of the Global Ocean Observing System. The Ssalto/Duacs altimeterproducts were produced and

24 distributed by the Copernicus Marine and Environment Monitoring Service (CMEMS)

25 (http://www.marine.copernicus.eu). The Microwave OI SST data are produced by Remote Sensing Systems and

26 sponsored by National Oceanographic Partnership Program (NOPP), the NASA Earth Science Physical

27 Oceanography Program, and the NASA MEaSUREs DISCOVER Project. Data are available at www.remss.com.

28 The chlorophyll_a version 6 is a remote dataset from the NASA Ocean Biology Processing Group (OBPG). The

29 OBPG is the official NASA data center that archives and distributes ocean color data

30 (http://oceancolor.gsfc.nasa.gov).

31

1   **References**
2
3   Bower, A. S., Armi, L., and Ambar, I.: Direct evidence of meddy formation off the southwestern coast of
4   Portugal, Deep Sea Research Part I: Oceanographic Research Papers, 42, 1621-1630, 1995.

5   Brandt, P., Bange, H. W., Banyte, D., Dengler, M., Didwischus, S. H., Fischer, T., Greatbatch, R. J., Hahn, J.,
6   Kanzow, T., Karstensen, J., Körtzinger, A., Krahmann, G., Schmidtko, S., Stramma, L., Tanhua, T., and
7   Visbeck, M.: On the role of circulation and mixing in the ventilation of oxygen minimum zones with a focus on
8   the eastern tropical North Atlantic, Biogeosciences, 12, 489-512, 2015.

9   Chaigneau, A., Eldin, G., and Dewitte, B.: Eddy activity in the four major upwelling systems from satellite
10   altimetry (1992–2007), Progress in Oceanography, 83, 117-123, 2009.

11   Chavez, F. P. and Messié, M.: A comparison of Eastern Boundary Upwelling Ecosystems, Progress in
12   Oceanography, 83, 80-96, 2009.

13   Chelton, D. B., Schlax, M. G., and Samelson, R. M.: Global observations of nonlinear mesoscale eddies,
14   Progress in Oceanography, 91, 167-216, 2011.

15   Chelton, D. B., Schlax, M. G., Samelson, R. M., and de Szoeke, R. A.: Global observations of large oceanic
16   eddies, Geophysical Research Letters, 34, L15606, doi:10.1029/2007GL030812, 2007.

17   Fiedler, B., Grundle, D., Schütte, F., Karstensen, J., Löscher, C. R., Hauss, H., Wagner, H., Loginova, A., Kiko,
18   R., Silva, P., and Körtzinger, A.: Oxygen Utilization and Downward Carbon Flux in an Oxygen-Depleted Eddy
19   in the Eastern Tropical North Atlantic, Biogeosciences Discuss., 2016, 1-35, 2016.

20   Fischer, G., Karstensen, J., Romero, O., Baumann, K. H., Donner, B., Hefter, J., Mollenhauer, G., Iversen, M.,
21   Fiedler, B., Monteiro, I., and Körtzinger, A.: Bathypelagic particle flux signatures from a suboxic eddy in the
22   oligotrophic tropical North Atlantic: production, sedimentation and preservation, Biogeosciences Discuss., 12,
23   18253-18313, 2015.

24   Hahn, J., Brandt, P., Greatbatch, R. J., Krahmann, G., and Körtzinger, A.: Oxygen variance and meridional
25   oxygen supply in the Tropical North East Atlantic oxygen minimum zone, Clim Dyn, doi: 10.1007/s00382-014-
26   2065-0, 2014. 1-26, 2014.

27   Hauss, H., Christiansen, S., Schütte, F., Kiko, R., Edvam Lima, M., Rodrigues, E., Karstensen, J., Löscher, C.
28   R., Körtzinger, A., and Fiedler, B.: Dead zone or oasis in the open ocean? Zooplankton distribution and
29   migration in low-oxygen modewater eddies, Biogeosciences Discuss., 12, 18315-18344, 2015.

30   J. Karstensen, F. Schütte, A. Pietri, G. Krahmann, B. Fiedler, C. Löscher, D. Grundle, H. Hauss, A. Körtzinger,
31   P. Testor, N. Vieira, and M. Visbeck: Isolation, mixing and nitrate budget of an oxygen depleted anticyclonic
32   modewater eddy, Biogeosciences Discuss., (this special issue), in prep., 2016
33
34   Karstensen, J., Fiedler, B., Schütte, F., Brandt, P., Körtzinger, A., Fischer, G., Zantopp, R., Hahn, J., Visbeck,
35   M., and Wallace, D.: Open ocean dead zones in the tropical North Atlantic Ocean, Biogeosciences, 12, 2597-
36   2605, 2015.
37
38   Karstensen, J., Stramma, L., and Visbeck, M.: Oxygen minimum zones in the eastern tropical Atlantic and
39   Pacific oceans, Progress in Oceanography, 77, 331-350, 2008.

40   Lachkar, Z. and Gruber, N.: A comparative study of biological production in eastern boundary upwelling
41   systems using an artificial neural network, Biogeosciences, 9, 293-308, 2012.

42   Löscher, C. R., Fischer, M. A., Neulinger, S. C., Fiedler, B., Philippi, M., Schütte, F., Singh, A., Hauss, H.,
43   Karstensen, J., Körtzinger, A., Künzel, S., and Schmitz, R. A.: Hidden biosphere in an oxygen-deficient Atlantic

1   open-ocean eddy: future implications of ocean deoxygenation on primary production in the eastern tropical
2   North Atlantic, Biogeosciences, 12, 7467-7482, 2015.

3   Luyten, J. R., Pedlosky, J., and Stommel, H.: The ventilated thermocline, Journal of Physical Oceanography, 13,
4   292-309, 1983.

5   Menkes, C. E., Kennan, S. C., Flament, P., Dandonneau, Y., Masson, S., Biessy, B., Marchal, E., Eldin, G.,
6   Grelet, J., and Montel, Y.: A whirling ecosystem in the equatorial Atlantic, Geophysical Research Letters, 29,
7   48-41-48-44, 2002.

8   Messié, M., Ledesma, J., Kolber, D. D., Michisaki, R. P., Foley, D. G., and Chavez, F. P.: Potential new
9   production estimates in four eastern boundary upwelling ecosystems, Progress in Oceanography, 83, 151-158,
10   2009.

11   Nencioli, F., Dong, C., Dickey, T., Washburn, L., and McWilliams, J. C.: A Vector Geometry–Based Eddy
12   Detection Algorithm and Its Application to a High-Resolution Numerical Model Product and High-Frequency
13   Radar Surface Velocities in the Southern California Bight, J Atmos Ocean Tech, 27, 564-579, 2010.

14   Pastor, M. V., Pelegrí, J. L., Hernández-Guerra, A., Font, J., Salat, J., and Emelianov, M.: Water and nutrient
15   fluxes off Northwest Africa, Continental Shelf Research, 28, 915-936, 2008.

16   Richardson, P. L., Price, J. F., Walsh, D., Armi, L., and Schröder, M.: Tracking Three Meddies with SOFAR
17   Floats, Journal of Physical Oceanography, 19, 371-383, 1989.

18   Schmidtko, S., Johnson, G. C., and Lyman, J. M.: MIMOC: A global monthly isopycnal upper-ocean
19   climatology with mixed layers, Journal of Geophysical Research: Oceans, 118, 1658-1672, 2013.

20   Schütte, F., Brandt, P., and Karstensen, J.: Occurrence and characteristics of mesoscale eddies in the tropical
21   northeast Atlantic Ocean, Ocean Sci. Discuss., 12, 3043-3097, 2015.

22   Stramma, L., Brandt, P., Schafstall, J., Schott, F., Fischer, J., and Körtzinger, A.: Oxygen minimum zone in the
23   North Atlantic south and east of the Cape Verde Islands, J Geophys Res-Oceans, 113, doi:
24   10.1029/2007JC004369, 2008.

25   Thomsen, S., Kanzow, T., Krahmann, G., Greatbatch, R. J., Dengler, M., and Lavik, G.: The formation of a
26   subsurface anticyclonic eddy in the Peru-Chile Undercurrent and its impact on the near-coastal salinity, oxygen
27   and nutrient distributions, Journal of Geophysical Research: Oceans, 2015. doi: 10.1002/2015JC010878, 2015.

28   von Schuckmann, K., Brandt, P., and Eden, C.: Generation of tropical instability waves in the Atlantic Ocean, J
29   Geophys Res-Oceans, 113, doi: 10.1029/2007JC004712, 2008.

30   Wyrtki, K.: The oxygen minima in relation to ocean circulation, Deep-Sea Res, 9, 11-23, 1962.

31   Zhang, Z., Zhang, Y., Wang, W., and Huang, R. X.: Universal structure of mesoscale eddies in the ocean,
32   Geophysical Research Letters, 40, 3677-3681, 2013.

33

2 **Tables**
3
4 **Table 1:** All available oxygen measurements below 40μmol kg^{-1} in the ETNA. The * indicates recent
5 observations which are not included in Fig. 4 due to not existent delayed time satellite products.

	Time	min O$_2$ between 0-200 m	Associated eddy type
11 Ship-Cruises: (81 profiles)			
Meteor 68/3	Summer 2006	17	CE
L'Atalante GEOMAR 3	Winter 2008	25	ACME
Meteor 80/2	Winter 2009	32	ACME
Meteor 83/1	Winter 2010	20	ACME
Meteor 96	Spring 2013	38	ACME
Meteor 97	Summer 2013	28	ACME
Islandia	Spring 2014	10	ACME
Meteor 105	Spring 2014	4	ACME
Meteor 116	Spring 2015	17	ACME*
Meteor 119	Autumn 2015	30	ACME*
Maria S. Merian 49	Winter 2015	35	CE*
9 Argo floats: (24 profiles)			
6900632	Autumn 2008	14	CE
1900652	Winter 2008	26	ACME
1900650	Summer 2009	27	ACME
1901360	Autumn 2014	34	CE
1901361	Autumn 2014	21	CE
1901362	Autumn 2014	26	CE
1901363	Autumn 2014	37	CE
1901364	Autumn 2014	24	ACME
1901365	Autumn 2014	24	ACME
4 Gliders: (32 profiles)			
IFM 11	Spring 2010	19	ACME
IFM 05	Summer 2013	9	CE
IFM 12	Winter 2014	1	ACME
IFM 13	Spring 2014	1	ACME
9 CVOO events: (36 profiles)			
Optode at 127 m depth	Winter 2007	15	ACME
Optode at 79 m depth	Autumn 2008	38	CE
Optode at 54 m depth	Winter 2010	2	ACME

Optode at 53 m depth	Winter 2012	17	ACME
Optode at 53 m depth	Spring 2012	30	CE
Optode at 45 m depth	Summer 2013	29	ACME
Optode at 45 m depth	Winter 2013	9	CE
Optode at 43 m depth	Winter 2015	2	ACME*
Optode at 43 m depth	Summer 2015	6	ACME*
∑ 173 profiles			**∑ 27 different eddies**

1   **Figures**
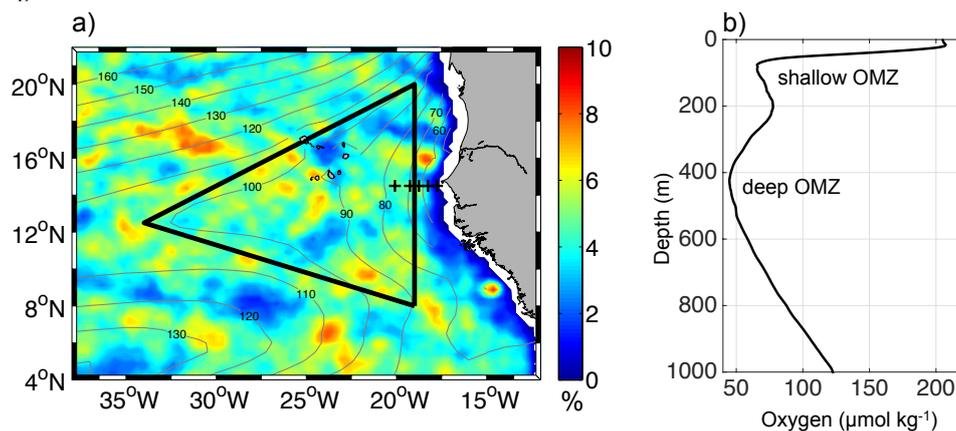
3
4   **Figure 1: a)** Map of the ETNA including contour lines of the oxygen minimum of the upper 200m (in µmol kg⁻

5   ¹) as obtained from the MIMOC climatology (Schmidtko et al., 2013). The color indicates the percentage of

6   "dead-zone" eddy coverage per year. The black triangle defines the SOMZ. The black crosses indicate the

7   position of the CTD stations of the research cruise M97, which are used to represent the vertical oxygen profile

8   shown on the right. **b)** mean vertical oxygen profile showing the shallow oxygen minimum centered around 80

9   m depths and the deep oxygen minimum centered at 450 m depth.
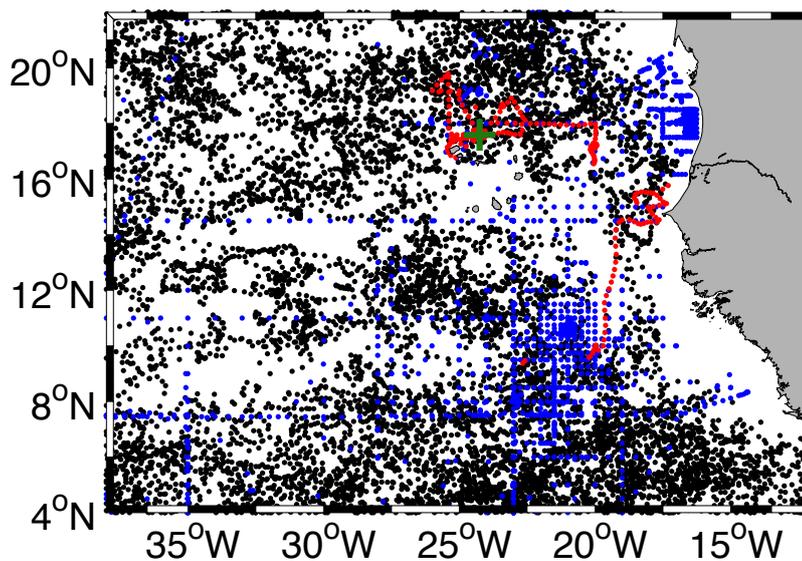
2
3 **Figure 2:** Map of ETNA containing all available profiles between 1998 and 2014. The green cross marks the
4 CVOO position, blue dots mark shipboard CTD stations, red dots mark the locations of glider profiles and black
5 dots locations of Argo float profiles.
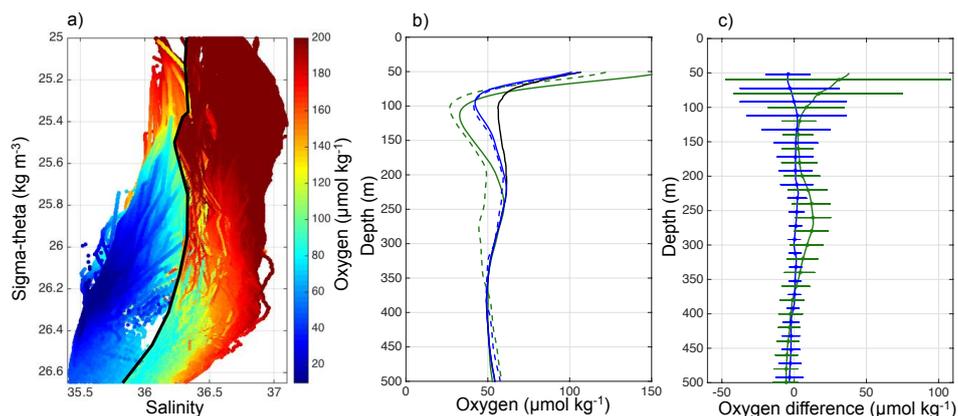
Figure 3: a) Salinity-σ_θ diagram with color indicating the oxygen concentrations. The black line separates the 173 profiles with minimum oxygen concentration of <40 µmol kg^{-1} (left side / more SACW characteristics) from profiles of the surrounding water (right side / more NACW characteristics), taken from the same devices shortly before and after the encounter with a low-oxygen eddy. **b)** Mean oxygen concentration versus depth of the coastal region (east of 18°W, solid black line), of all CEs (solid blue line) and all ACMEs (solid green line) with available oxygen measurements. The dashed line represents the reconstructed mean oxygen concentration for the same CEs (blue) and ACMEs (green). **c)** Difference between the reconstructed and measured oxygen concentrations in CEs (blue) and ACMEs (green) with associated standard deviation (horizontal lines).
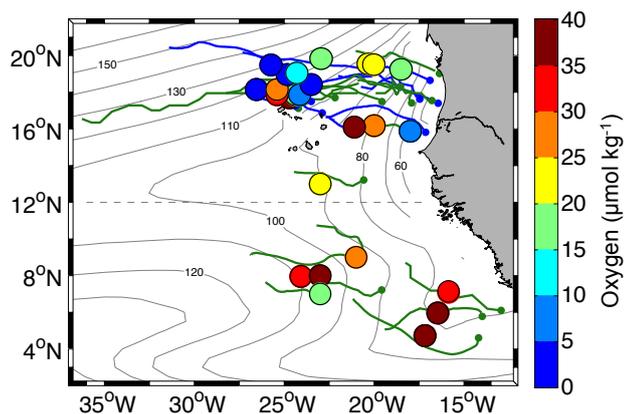
Figure 4: Minimum oxygen concentration (contour lines, µmol kg^{-1}) in the tropical Northeast Atlantic Ocean between the surface and 200 m depth as obtained from the MIMOC climatology (Schmidtko et al., 2013). Superimposed colored dots are all low oxygen measurements (below 40 µmol kg^{-1} in the upper 200 m) which could be associated with eddy-like structures. The size of the dots represents a typical size of the mesoscale eddies. The associated trajectories of the eddies are shown in green for ACMEs and in blue for cyclones. The oxygen concentrations are from the combined dataset of shipboard, mooring, glider and Argo float measurements.
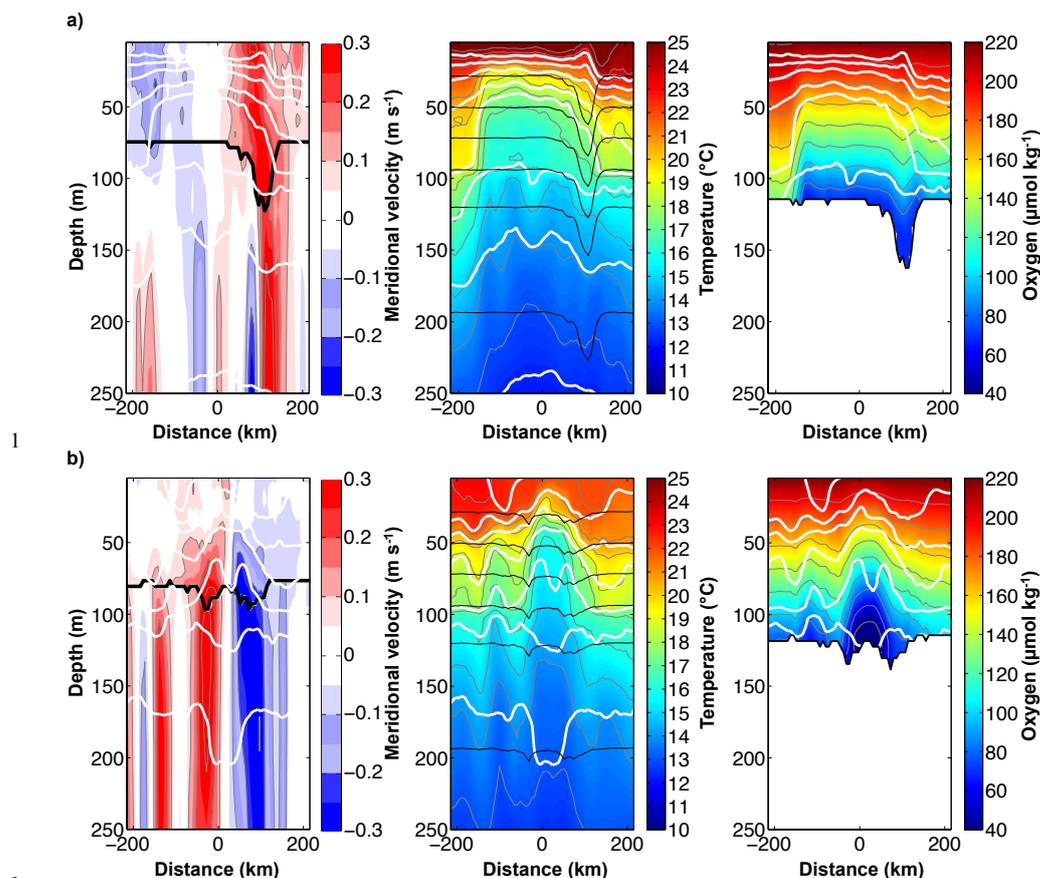
Figure 5: Meridional velocity, temperature and oxygen of an exemplary **a)** CE and **b)** ACME at the CVOO mooring. Both eddies passed the CVOO on a westward trajectory with the eddy center north of the mooring position (CE 20 km, ACME 13 km). The CE passed the CVOO from October to December 2006 and the ACME between January and March 2007. The thick black lines in the velocity plots indicate the position of an upward looking ADCP. Below that depth calculated geostrophic velocity is shown. The white lines represent density surfaces inside the eddies and the thin grey lines isolines of temperature and oxygen, respectively. Thin black lines in the temperature and oxygen plot mark the vertical position of the measuring devices. For the oxygen plot saturation at the surface is assumed and data is linearly interpolated between the measuring device and surface.
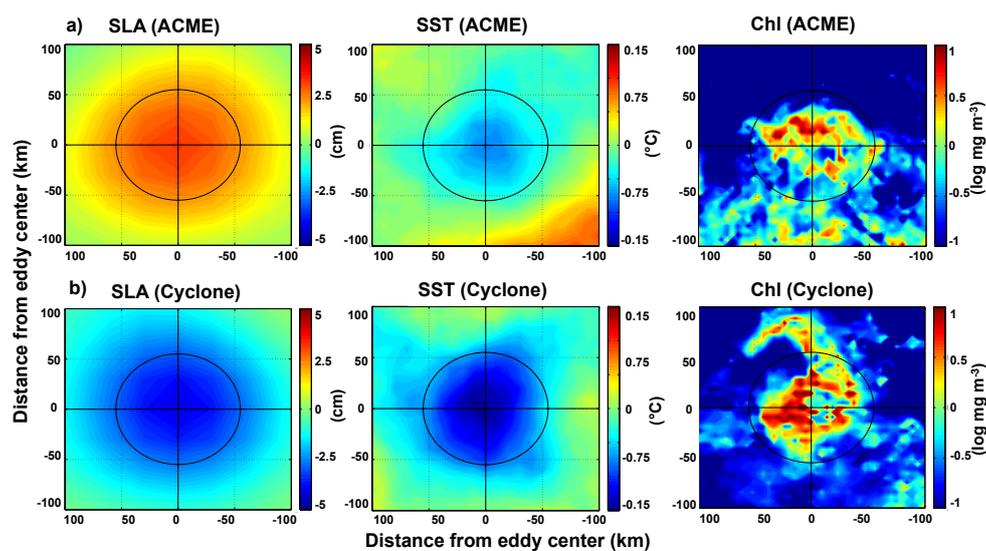
3 **Figure 6:** Composites of surface signature for SLA, SST and Chl from all detected "dead-zone" eddies: **a)**

4 ACMEs and **b)** cyclones. The solid black cross marks the eddy center and the solid black circle the average

5 radius. Due to significant cloud cover the number of Chl data are much less when compared the SLA and SST

6 data, thus there is more lateral structure.
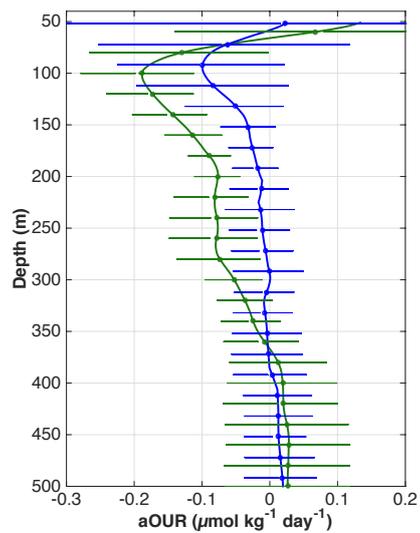
Figure 7: Depth profiles of a mean apparent oxygen utilization rate (aOUR, μmol kg^{-1} d^{-1}) within CEs (blue) and

ACMEs (green) with associated standard deviation (horizontal lines).
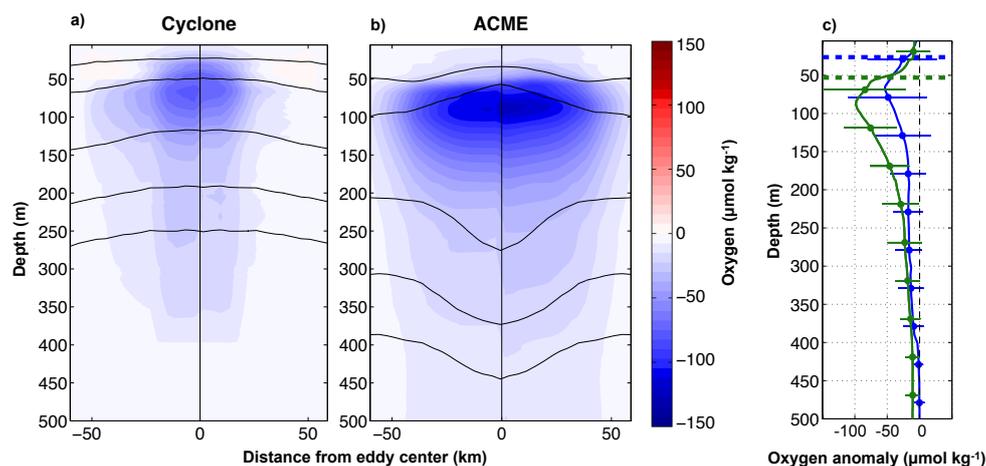
Figure 8: Vertical structure of oxygen from the composite **a)** CE and **b)** ACME in the ETNA presented as a half section across the eddies. The left side of each panel (-60 to 0 km) is based on reconstructed and measured oxygen profiles whereas the right side (0 to 60 km) is based on measured oxygen profiles only. The grey lines represents the density surfaces inside the eddies. **c)** Mean profiles of the oxygen anomalies based on measured profiles only, green colors are associated to ACMEs and blue to CEs. The thick dashed line indicates the mean ML within the different eddy types. The horizontal lines indicate the standard deviation at that point. The grey vertical dashed line represents zero oxygen.
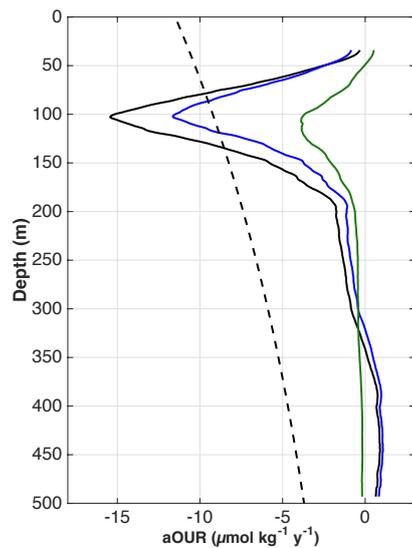
2   **Figure 9:** Depth profile of apparent oxygen utilization rate (aOUR, µmol kg^{-1} y^{-1}) for the Atlantic as published

3   from Karstensen et al. (2008) (dashed black line), the oxygen consumption profile due to "dead-zone" eddies in

4   the SOMZ (solid black line) and the separation into CEs (blue) and ACMEs (green).